Optical Forces Arising from Phase Gradients

Yohai Roichman,[1] Bo Sun,[2] Yael Roichman,[1] Jesse Amato-Grill,[1] and David G. Grier[1]

[1]*Department of Physics and Center for Soft Matter Research, New York University, New York, New York 10003, USA*
[2]*Department of Chemistry and Center for Soft Matter Research, New York University, New York, New York 10003, USA*

(Received 26 July 2007; published 8 January 2008)

We demonstrate both theoretically and experimentally that phase gradients in a light field can be used to create a new category of optical traps complementary to the more familiar intensity-gradient traps known as optical tweezers. We further show that the work done by phase-gradient forces is path dependent and briefly discuss some ramifications of this nonconservativity.

DOI: 10.1103/PhysRevLett.100.013602 PACS numbers: 37.10.Vz, 42.40.Jv, 82.70.Dd, 87.80.−y

Light's ability to exert forces has been recognized since Kepler's *De Cometis* of 1619 described the deflection of comet tails by the sun's rays. Maxwell showed that the momentum flux in a beam of light is proportional to the intensity and can be transferred to illuminated objects, resulting in radiation pressure that pushes objects along the direction of propagation. This Letter demonstrates that *phase* gradients can redirect radiation pressure to create optical force fields transverse to the optical axis. Photon orbital angular momentum (OAM) [1] is one experimentally realized [2,3] example of this phenomenon. We then put phase-gradient forces to work by combining them with intensity gradients in holographically projected light fields to create a new category of extended optical traps with tailored force profiles.

The vector potential describing a beam of light of frequency ω and polarization $\hat{\boldsymbol{\varepsilon}}(\boldsymbol{r})$ may be written as

$$\boldsymbol{A}(\boldsymbol{r}, t) = u(\boldsymbol{r}) e^{i\Phi(\boldsymbol{r})} e^{-i\omega t} \hat{\boldsymbol{\varepsilon}}(\boldsymbol{r}), \tag{1}$$

where $u(\boldsymbol{r})$ is the real-valued amplitude and $\Phi(\boldsymbol{r})$ is the real-valued phase. We assume for simplicity that the light is linearly polarized so that $\hat{\boldsymbol{\varepsilon}}(\boldsymbol{r})$ is real. For a plane wave propagating in the $\hat{z}$ direction, $\Phi(\boldsymbol{r}) = kz$, where $k = n_m \omega / c$ is the light's wave number, c is the speed of light in vacuum, and n_m is the refractive index of the medium. Imposing a transverse phase profile $\varphi(\boldsymbol{r})$ on the wavefronts of such a beam yields

$$\Phi(\boldsymbol{r}) = k_z(\boldsymbol{r}) z + \varphi(\boldsymbol{r}), \tag{2}$$

where $\hat{z} \cdot \boldsymbol{\nabla} \varphi = 0$. The direction of the wave vector, $\boldsymbol{k}(\boldsymbol{r}) = k_z(\boldsymbol{r})\hat{z} + \boldsymbol{\nabla}\varphi$, now varies with position, subject to the constraint $k^2 = |\boldsymbol{k}|^2 = k_z^2 + |\boldsymbol{\nabla}\varphi|^2$, which applies in the paraxial limit, $k \gg |\boldsymbol{\nabla}\varphi|$. The associated electric and magnetic fields are given in the Lorenz gauge by

$$\boldsymbol{E}(\boldsymbol{r}, t) = -\frac{\partial}{\partial t} \boldsymbol{A}(\boldsymbol{r}, t) \quad \text{and} \quad \boldsymbol{H}(\boldsymbol{r}, t) = \frac{1}{\mu} \boldsymbol{\nabla} \times \boldsymbol{A}(\boldsymbol{r}, t), \tag{3}$$

where μ is the magnetic permeability of the medium, which we assume to be homogeneous and isotropic. Following Abraham's formulation [4], the momentum flux carried by the beam is

$$\boldsymbol{g}(\boldsymbol{r}) = \frac{1}{c^2} \operatorname{Re}\{\boldsymbol{E}^* \times \boldsymbol{H}\} = \frac{k}{n_m \mu c} I(\boldsymbol{r}) \boldsymbol{\nabla} \Phi, \tag{4}$$

where $I(\boldsymbol{r}) = |u(\boldsymbol{r})|^2$ is the light's intensity, and where we have employed the gauge condition $\boldsymbol{\nabla} \cdot \boldsymbol{A} = 0$.

The momentum flux separates into an axial component $\boldsymbol{g}_z(\boldsymbol{r}) = k k_z I(\boldsymbol{r}) (n_m \mu c)^{-1} \hat{z}$ and

$$\boldsymbol{g}_\perp(\boldsymbol{r}) = \frac{k}{n_m \mu c} I(\boldsymbol{r}) \boldsymbol{\nabla} \varphi \tag{5}$$

transverse to the optical axis [5], which is responsible for transverse forces.

More than a decade ago, Allen and co-workers [1] pointed out that the helical phase profile, $\varphi(\boldsymbol{r}) = \ell\theta$, imbues a beam of light with an OAM flux, $\boldsymbol{r} \times \boldsymbol{g}_\perp$, amounting to $\ell\hbar$ per photon. Here, θ is the azimuthal angle around the optical axis, and ℓ is an integer describing the wave fronts' helical pitch. This OAM is distinct from the photons' intrinsic spin angular momentum [6,7]. Through it, even linearly polarized light can exert a torque around the optical axis [2,8]. Equation (5) reveals this to be a manifestation of the more general class of transverse forces arising from phase gradients.

Intensity gradients also exert forces on illuminated objects [9]. In this case, the dipole moment induced in the object responds to gradients in the field, yielding a force proportional to the gradient of the intensity, which therefore is manifestly conservative [10]. For a small sphere of radius a, the intensity-gradient force has the form [9,11],

$$\boldsymbol{F}_\nabla(\boldsymbol{r}) = n_m \frac{k^2 a^3}{2} \left(\frac{m^2 - 1}{m^2 + 2} \right) \nabla I, \tag{6}$$

where $m = n_p / n_m$ is the ratio of the particle's refractive index, n_p, to the medium's, n_m. Unlike $\boldsymbol{g}$, $\boldsymbol{F}_\nabla$ can be directed up the optical axis. The resulting axial restoring force is the basis of single-beam optical traps [9].

Because beams of light have gradients in both the intensity and the phase, the total optical force is not conservative. This is evident because

 © 2008 The American Physical Society

$$\nabla \times \boldsymbol{g} = \frac{k}{\mu n_m}(\nabla I) \times (\nabla \Phi) \tag{7}$$

does not vanish in general. Although Ashkin pointed out that optical traps exert nonconservative forces [10], subsequent reports have treated optical tweezers as (conservative) potential energy wells.

We realize phase-gradient forces using a new class of extended optical traps created through shape-phase holography [12–15]. Our apparatus, shown schematically in Fig. 1(a), uses a phase-only spatial light modulator (SLM) (Hamamatsu X8267-16) to imprint computer-generated holograms on a laser beam (Coherent Verdi 5W) at a vacuum wavelength of 532 nm. The modified beam is relayed to an objective lens (Nikon Plan Apo, 100 × oil immersion, with a numerical aperture of 1.4) that focuses it into the intended three-dimensional optical trapping pattern. A beam splitter reflects the laser light into the objective's input pupil while allowing images at other wavelengths to pass through to a video camera (NEC TI-324AII).

The holograms designed for this study bring laser light to a focus along one-dimensional curves, C, embedded in the three-dimensional focal volume of the objective lens. Each hologram also encodes a designated intensity profile $I(s)$ and phase profile $\varphi(s)$ along the arclength s of C. This is accomplished by numerically back-projecting [16] the desired field along C onto the plane of the SLM to obtain the ideal complex-valued hologram, $\psi(\boldsymbol{r}) = |b(\boldsymbol{r})| \exp(ip(\boldsymbol{r}))$. The shape-phase algorithm [12–14] assigns the phase shifts $p(\boldsymbol{r})$ to the SLM's pixels with a probability proportional to $|b(\boldsymbol{r})|$. An alternate phase pattern imprinted on the unassigned pixels diverts excess light away from C [12].

The images in Figs. 1(b) and 1(c) show a focused line trap [12] and ring trap [14], respectively, each designed to have uniform intensity and phase gradients. These images were obtained by placing a mirror in the microscope's focal plane and imaging the reflected light [13]. Because the holograms come to a diffraction-limited focus, their axial intensity gradients are steep enough to trap particles in three dimensions [9]. To study the phase-gradient force predicted by Eq. (5), we track [17] colloidal spheres moving along these traps.

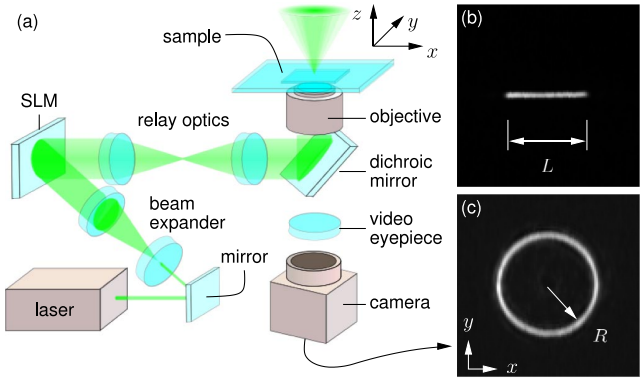

FIG. 1 (color online). (a) Schematic representation of the optimized holographic optical trapping system using shape-phase holography to project extended optical traps. (b) Experimental realization of a holographic line trap carrying a phase gradient in the $\hat{\boldsymbol{x}}$ direction, imaged in the plane of best focus. (c) Focal pattern of a holographic ring trap with $\ell = 30$.

In the case of the line trap, we first subjected the trapped particle to linear phase gradients, $\nabla\varphi = q\hat{\boldsymbol{x}}$, over the range $q = \pm 12$ radians/μm. The insets to Fig. 2 show axial sections through volumetric reconstructions of the trap's three-dimensional intensity distribution [13] for two different values of q. The diffraction-limited focal line remains in the xy plane despite the imposed phase gradient. The beam's direction of propagation, however, deviates from $\hat{\boldsymbol{z}}$ by the angle $\sin^{-1}(q/k)$. This tilt directs a component of the beam's radiation pressure along $\hat{\boldsymbol{x}}$. The images in Fig. 2 confirm the phase gradients' magnitude and uniformity.

The line trap was projected into an aqueous dispersion of colloidal silica spheres $2a = 1.53$ μm in diameter sealed into the 40 μm thick gap between a glass microscope slide and a no. 1 glass coverslip. Focusing the trap near the sample's midplane avoids reflections from the glass-water interface and minimizes hydrodynamic coupling to the walls. Equation (5) and the Stokes mobility law for a colloidal sphere then suggest that a trapped particle's speed, v, should be proportional to q.

To test this prediction, we measured the time required for a single sphere to travel the length, $L = 5$ μm, of a 100 mW trap as the sign of q was flipped 20 times for each value of $|q|$. The observed root-mean-square off-line excursions of roughly 200 nm suggest axial and lateral trap stiffnesses comparable to those of a pointlike optical tweezer powered by 1 mW. Under these conditions, the trapped sphere traveled along the line at speeds up to 2 μm/s when subjected to the largest phase gradients.

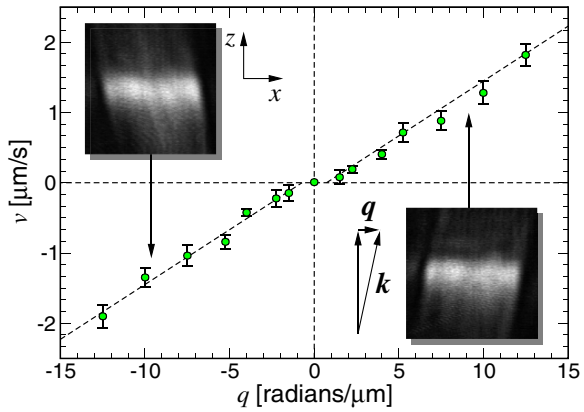

FIG. 2 (color online). Dependence of mean velocity v on phase-gradient q. Insets: Axial slices in the xz plane through the line trap's three-dimensional intensity distribution at two values of q.

Results obtained by systematically varying q are plotted in Fig. 2. They show the anticipated linear dependence, except very near $q = 0$, where phase-gradient forces are too weak to overcome localized pinning centers created by small uncorrected intensity variations.

More complicated phase gradients give rise to more interesting physical effects. The particles shown in Fig. 3 also are trapped along a uniformly bright line trap of length $L = 10\ \mu$m. This line, however, has a parabolic phase profile, $\varphi(x) = \pm(qx)^2$, that is predicted to force objects either out to the ends of the line or toward its center depending on the sign. The images in Figs. 3(a) and 3(b) demonstrate both effects for a pair of trapped colloidal spheres. Axial sections through the three-dimensional intensity distribution show that the phase-gradient barrier results from light diverging along the line's length, while the well results from the projection of converging rays. So long as the particles are rigidly confined to the uniformly bright focal line, Eq. (7) suggests that the phase-gradient force approximates a conservative potential energy landscape.

Like holographic line traps, holographic ring traps, such as the example in Fig. 1(c), can be endowed with arbitrary phase profiles, including the uniform azimuthal phase gradient, $\varphi(\boldsymbol{r}) = \ell\theta$, that defines a helical mode. A helical profile, by itself, causes a beam to focus into a ring of light, forming a torque-exerting optical trap known as an optical vortex [2]. Whereas the radius of an optical vortex, R_ℓ, is proportional to its helicity [7,18], holographic ring traps can be projected with any desired radius, R, independent of ℓ [14]. This facilitates systematic studies of colloidal transport under varying phase gradients. Also unlike optical vortices, holographic ring traps have strong enough axial intensity gradients to trap objects in three dimensions. This can be seen in the computed axial section in Fig. 4(a) in which the trap appears as two bright focal spots on the midline. Imposing a helical phase profile on a ring trap suppresses the beam's axial intensity through destructive interference, diverting it instead to a radius, R_ℓ from the axis [7,18]. If the ring's radius R exceeds the vortices', R_ℓ, the converging helical beam focuses not only to the intended ring trap, but also to two conventional optical vortices above and below the focal plane, which appear as bright features in Fig. 4(a). This structure also is evident in the ring trap's measured three-dimensional intensity field [13] in Fig. 4(b). The optical vortices' comparatively weak axial intensity gradients are evident in Fig. 4(a).

A ring trap with a uniform azimuthal phase gradient exerts a torque about its axis. We demonstrated this by tracking a colloidal silica sphere circulating around a holographic ring trap of radius $R = 2.6\ \mu$m projected into the midplane of a 40 μm thick sample. The trapped particle was subjected to azimuthal phase gradients in the range $\ell = \pm 50$, and its peak speed was measured [17] to within 10% for each value of the helicity. The results are plotted in Fig. 4.

Like optical vortices, holographic ring traps carrying orbital angular momentum are subject to ℓ-fold and 2ℓ-fold azimuthal intensity variations due to nonideal phase scaling [19] that trap the particle for $|\ell| < \ell_c$ [7,20]. For $|\ell| > \ell_c$, however, the particle's peak speed

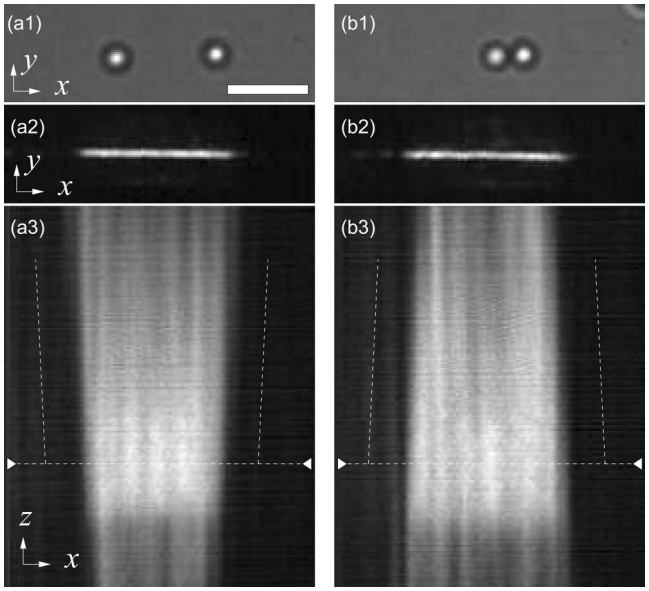

FIG. 3. (a) Phase-gradient barrier and (b) phase-gradient well in a uniformly bright line trap. (1) Two 1.5 μm diameter silica spheres trapped on the line. (2) The uniform in-plane intensity of the focused line. (3) Axial section through the measured intensity, showing the divergence (a3) and convergence (b3) due to the phase profile. Scale bar indicates 5 μm.

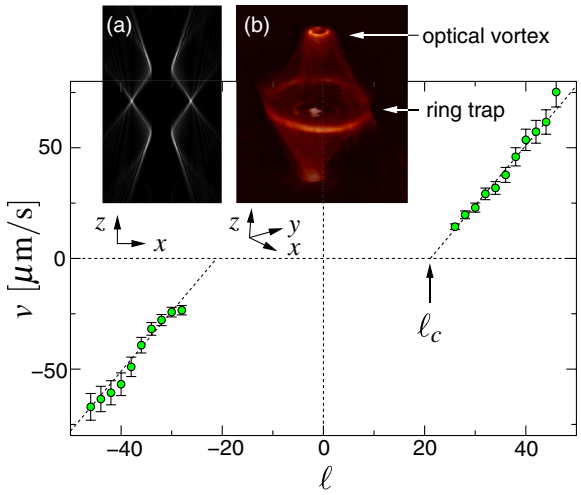

FIG. 4 (color online). Colloidal transport driven by azimuthal phase gradients in holographic ring traps. (a) Computed axial section through a holographic ring trap of radius $R = 20\ \mu$m and helicity $\ell = 30$. (b) Volumetric representation of the measured three-dimensional intensity field in a holographic ring trap of radius $R = 20\ \mu$m and $\ell = 10$. Data points show the peak speed v of a single colloidal silica sphere circulating around the ring in (b) as a function of topological charge ℓ.

increases linearly with $|\ell|$, consistent with the predictions of Eq. (5). Intermittent circulation near $|\ell| = \ell_c$ gives rise to large velocity fluctuations characterized by giant enhancement of the particle's effective diffusion coefficient [20]. Disorder in the effective force landscape also gives rise to interesting collective dynamics for multiple particles trapped on the ring, including transitions among periodic, chaotic and weakly chaotic steady states [21]. Phase-gradient forces in holographic ring traps therefore provide useful model systems for studying fundamental problems in nonequilibrium statistical mechanics. They also promise practical applications as the basis for microscopic pumps [22], mixers [23], and optomechanical micromachines [24]. Azimuthal phase gradients also can be used to endow a holographic ring trap with more complicated force profiles, even if the ring's intensity is uniform.

We have demonstrated that phase gradients in a beam of light give rise to forces transverse to the optical axis, and that these forces can be harnessed for novel optical traps. A well-established example, photon OAM in helical modes, is shown to be a particular manifestation of this general effect. Tuning optical traps' force profiles with phase gradients will be useful for manipulating microscopic objects, and will greatly facilitate rapid measurements of colloidal interactions, for example. Although phase-gradient forces generally are nonconservative, they can act as conservative force fields on appropriately restricted manifolds. More generally, optical forces' nonconservativity may engender interesting effects in illuminated particles' dynamics, including departures from Boltzmann statistics for systems nominally in equilibrium. Finally, we note in passing that phase gradients give rise to spatial variations in the polarization, which we have not considered in this Letter. Although optically isotropic materials are not influenced by polarization gradients, anisotropic materials can be. Phase-directed polarization gradients therefore should provide additional independent avenues for controlling microscopic systems.

This work was supported by the National Science Foundation through Grant No. DMR-0606415. We are grateful to Marco Polin for enlightening conversations.

[1] L. Allen, M. W. Beijersbergen, R. J. C. Spreeuw, and J. P. Woerdman, Phys. Rev. A **45**, 8185 (1992).

[2] H. He, N. R. Heckenberg, and H. Rubinsztein-Dunlop, J. Mod. Opt. **42**, 217 (1995); K. T. Gahagan and G. A. Swartzlander, Opt. Lett. **21**, 827 (1996); N. B. Simpson, L. Allen, and M. J. Padgett, J. Mod. Opt. **43**, 2485 (1996).

[3] J. E. Curtis and D. G. Grier, Opt. Lett. **28**, 872 (2003); S. Tao, X.-C. Yuan, J. Lin, X. Peng, and H. Niu, Opt. Express **13**, 7726 (2005); J. Lin, X.-C. Yuan, S. H. Tao, X. Peng, and H. B. Niu, Opt. Express **13**, 3862 (2005); C. H. J. Schmitz, K. Uhrig, J. P. Spatz, and J. E. Curtis, Opt. Express **14**, 6604 (2006).

[4] R. Loudon, Fortschr. Phys. **52**, 1134 (2004).

[5] A. Nisbet and E. Wolf, Proc. Cambridge Philos. Soc. **50**, 614 (1954).

[6] N. B. Simpson, K. Dholakia, L. Allen, and M. J. Padgett, Opt. Lett. **22**, 52 (1997); L. Allen, M. J. Padgett, and M. Babiker, Prog. Opt. **39**, 291 (1999); A. T. O'Neil and M. J. Padgett, Opt. Commun. **185**, 139 (2000); A. T. O'Neil, I. MacVicar, L. Allen, and M. J. Padgett, Phys. Rev. Lett. **88**, 053601 (2002).

[7] J. E. Curtis and D. G. Grier, Phys. Rev. Lett. **90**, 133901 (2003).

[8] H. He, M. E. J. Friese, N. R. Heckenberg, and H. Rubinsztein-Dunlop, Phys. Rev. Lett. **75**, 826 (1995); M. E. J. Friese, J. Enger, H. Rubinsztein-Dunlop, and N. R. Heckenberg, Phys. Rev. A **54**, 1593 (1996).

[9] A. Ashkin, J. M. Dziedzic, J. E. Bjorkholm, and S. Chu, Opt. Lett. **11**, 288 (1986).

[10] A. Ashkin, Biophys. J. **61**, 569 (1992).

[11] Y. Harada and T. Asakura, Opt. Commun. **124**, 529 (1996).

[12] Y. Roichman and D. G. Grier, Opt. Lett. **31**, 1675 (2006).

[13] Y. Roichman, I. Cholis, and D. G. Grier, Opt. Express **14**, 10907 (2006).

[14] Y. Roichman and D. G. Grier, Proc. SPIE-Int. Soc. Opt. Eng. **6483**, 64830F (2007).

[15] E. R. Dufresne and D. G. Grier, Rev. Sci. Instrum. **69**, 1974 (1998); D. G. Grier, Nature (London) **424**, 810 (2003); M. Polin, K. Ladavac, S.-H. Lee, Y. Roichman, and D. G. Grier, Opt. Express **13**, 5831 (2005); Y. Roichman, A. S. Waldron, E. Gardel, and D. G. Grier, Appl. Opt. **45**, 3425 (2006).

[16] J. W. Goodman, *Introduction to Fourier Optics* (McGraw-Hill, New York, 2005), 3rd ed.

[17] J. C. Crocker and D. G. Grier, J. Colloid Interface Sci. **179**, 298 (1996).

[18] S. Sundbeck, I. Gruzberg, and D. G. Grier, Opt. Lett. **30**, 477 (2005).

[19] S.-H. Lee and D. G. Grier, Opt. Express **13**, 7458 (2005).

[20] S.-H. Lee and D. G. Grier, Phys. Rev. Lett. **96**, 190601 (2006).

[21] Y. Roichman, G. M. Zaslavsky, and D. G. Grier, Phys. Rev. E **75**, 020401(R) (2007).

[22] K. Ladavac and D. G. Grier, Opt. Express **12**, 1144 (2004).

[23] J. E. Curtis, B. A. Koss, and D. G. Grier, Opt. Commun. **207**, 169 (2002).

[24] K. Ladavac and D. G. Grier, Europhys. Lett. **70**, 548 (2005).